Membrane-mediated ligand unbinding of the PK-11195 ligand from the translocator protein (TSPO)

Tom Dixon[1,2], Arzu Uyar[2], Shelagh Ferguson-Miller[2], and Alex Dickson[1,2,✉]

[1]Department of Computational Mathematics, Science and Engineering, Michigan State University, East Lansing, USA
[2]Department of Biochemistry & Molecular Biology, Michigan State University, East Lansing, USA

The translocator protein (TSPO), previously known as the peripheral benzodiazepine receptor, is of longstanding medical interest as both a biomarker for neuroinjury and a potential drug target for neuroinflammation and other disorders. Recently it was shown that ligand residence time is a key factor determining steroidogenic efficacy of TSPO-binding compounds. This spurs interest in simulations of (un)binding pathways of TSPO ligands, which could reveal the molecular interactions governing ligand residence time. In this study, we use a weighted ensemble algorithm to determine the unbinding pathway for different poses of PK-11195, a TSPO ligand used in neuroimaging. In contrast with previous studies, our results show that PK-11195 does not dissociate directly into solvent but instead dissociates via the lipid membrane by going between the transmembrane helices. We analyze this path ensemble in detail, constructing descriptors that can facilitate a general understanding of membrane-mediated ligand binding.

Correspondence: ***alexrd @msu.edu***

The binding affinity of a ligand to its protein target has long been viewed as the key parameter determining its efficacy. However, recent studies have shown that in some protein-ligand systems residence time (RT) correlates more strongly with efficacy than binding affinity (1). Unlike the binding affinity, RT is not a state function; it depends on the height of the free energy barrier separating the bound and unbound states. In order to rationally design ligands for longer RTs we need to understand the (un)binding mechanisma nd what molecular interactions occur along the ligand (un)binding pathway (2–4).

Previous studies have shown that the translocator protein 18kDa (TSPO) is one such protein where RT is important for predicting efficacy (5). TSPO is a well-conserved membrane protein, being present all kingdoms including prokaryotes as well as in the outer mitochondrial membrane of eukaryotes (6). TSPO has five transmembrane α-helices (TM1-5) along with a small helical region in a 20-residue loop connecting TM-1 and TM-2 on the cytosolic side (Fig. 1A). While in the membrane, TSPO is largely found in a dimeric state (7). To date, four different structures have been solved for TSPO structures from both bacterial (7, 8) and mammalian (9, 10) organisms the former by X-Ray crystallography, the latter by NMR.

While the structure of TSPO have been solved, its function remains unknown. In humans, TSPO is highly expressed in steroidogenic tissues, leading to the hypothesis that it is involved in the regulation of cholesterol transport across the mitochondrial membrane; indeed, TSPO has been shown to have a high binding affinity for cholesterol (11). There are other studies linking it to apoptosis (12, 13) and cellular stress regulation in TSPO knockout mice (14, 15), although evidence for this is mixed (16, 17). Increased TSPO expression has also been observed in cases of neurodegenerative diseases such as Alzheimer's and Parkinson's diseases (18). Relatedly, due to its high expression in areas of inflammation TSPO serves as a biomarker for neurodegenerative disease and brain trauma, and radiolabeled ligands such as [H3]-PK-11195, are commonly used in positron emission tomography (PET) scans (19). PK-11195 (hereafter denoted "PK") is an isoquinoline carboxamide with no known therapeutic effect (17) and a RT of 34 min (5, 20).

Molecular dynamics (MD) simulations have been previously performed using a bound TSPO-PK complex. Researchers recently determined the unbinding pathway of PK from a rat TSPO model generated from the PDB 2MGY structure (21). To generate unbinding paths they used a combination of random accelerated MD (RAMD) and steered MD (SMD) and determined that PK unbinds into the cytosol through the largely disordered LP1 region. Unfortunately, this starting structure, determined by NMR, was significantly destabilized by the detergent used in the purification (22) (23). Also, the methods used to determine the unbinding pathway (RAMD) have the potential to impart bias on the predicted (un)binding path, as they affect the kinetics of transition between microstates along the path. Another group performed an induced-fit docking of PK using Glide (24) with a homology model to resemble the mammalian (mouse) TSPO structure using the PDB 4UC1 *Rhodobacter sphaeroides* structure. They simulated the TSPO-PK complex for 700 ns and did not observe significant ligand displacement, which is expected due to the extremely long RT of the TSPO-PK complex.

Here we study the unbinding mechanism for the TSPO-PK complex, using PDB 4UC1 as the TSPO starting structure (7) and using a weighted ensemble algorithm: Resampling of Ensembles by Variation Optimization (REVO) to generate continuous unbinding pathways without perturbing the underlying dynamics (25). This algorithm performs MD on many trajectories (walkers) in parallel and performs "merg-

ing" and "cloning" operations on the walkers to increase sampling in under-explored regions. REVO chooses trajectories for cloning and merging using an objective function that is based on the distances between walkers: outliers, with large distances to other walkers, are chosen for cloning, and other, more central walkers are chosen for merging (more details in SI S1.4). In weighted ensemble algorithms, each walker is assigned a statistical weight, which is divided upon cloning and summed upon merging, allowing for the direct calculation of observables as weighted averages of trajectory properties. REVO has been previously applied to study ligand unbinding on a series of host-guest systems (26) and the trypsin-benzamidine system (25).

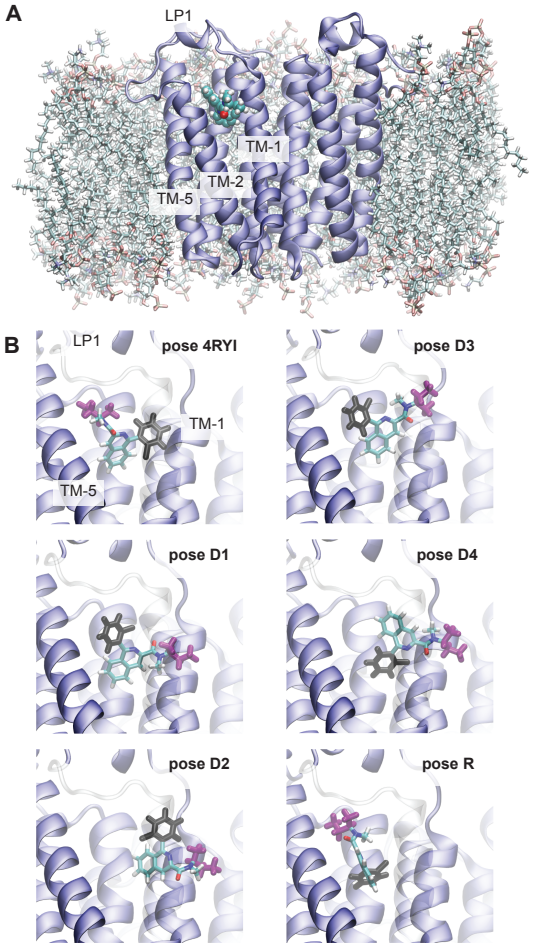

Fig. 1. TSPO-PK11195 system. (A) Front view of the TSPO dimer in the membrane with PK bound. (B) All six starting poses are shown from the side view, along the inter-dimer axis. To compare poses, two moeities of PK are colored in black (o-chlorophenyl) and magenta (1-methylpropyl), with the rest of the molecule colored according to atom name. TM-2 is shown as transparent for clarity.

We comprehensively studied the TSPO-PK interaction landscape using a set of REVO simulations initialized at six different starting poses (Fig. 1B). Pose 4RYI copies the PK orientation from the PDB 4RYI structure (8), and Poses D1-D4 were constructed by docking PK into 4UC1 using Schrödinger Glide (27). Pose R was determined previously by Xia *et al.* (28). by docking PK into an mTSPO structural ensemble made from PDB 2MGY, 4RYI, and 4UC2 structures (7). All six poses were then used to initialize otherwise identical systems comprised of the TSPO dimer in its 4UC1 structure, a lipid membrane, 0.15 M KCl and solvated with TIP3 waters using CHARMM-GUI (29) (see SI S1.1-S1.3). Each pose was simulated using three independent REVO simulations with 48 walkers each and 1200 cycles of dynamics and resampling, resulting in a total simulation time of 5.18 μs per pose (31.1 μs total).

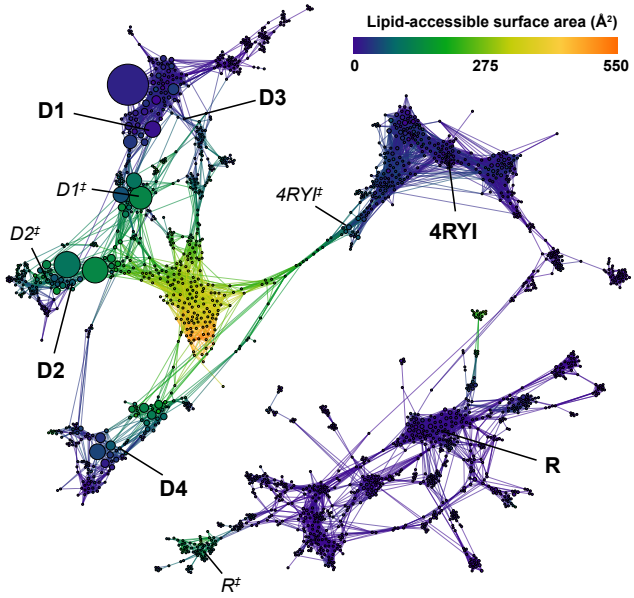

Fig. 2. Combined conformation space network of all REVO simulations from each starting pose. Each node in the network represents a cluster of ligand poses, and are sized according to the cluster weight. Nodes are connected by edges if the ligand poses are observed to interconvert in the REVO trajectory segments. Nodes are colored according to the lipid-accessible surface area (LASA). Starting poses are marked in bold and transition state poses shown in Fig. 4D are marked in italics.

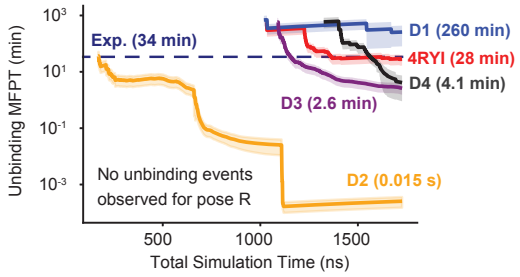

Fig. 3. Convergence of mean first passage time (MFPT) estimates as a function of simulation time is shown for each starting pose. The light shaded area shows the standard error across the three simulations conducted for each pose. The experimental MFPT of 34 min is shown as a dashed line.

After the MD simulations were completed, all frames were clustered together into a conformational space network (CSN) shown in Fig. 2, where each node represents a PK pose (see SI S1.7) and the edges reveal which poses interconvert in our simulations. All of the starting poses form a connected network, though pose R is only connected via a couple of low probability edges to the pose 4RYI ensemble (Fig. S2). The 4RYI pose is similarly connected to pose D4, but is also connected to the other docked poses via the high lipid accessible surface area (LASA) clusters.

Unlike in the Bruno *et al.* study (21), PK did not dissoci-

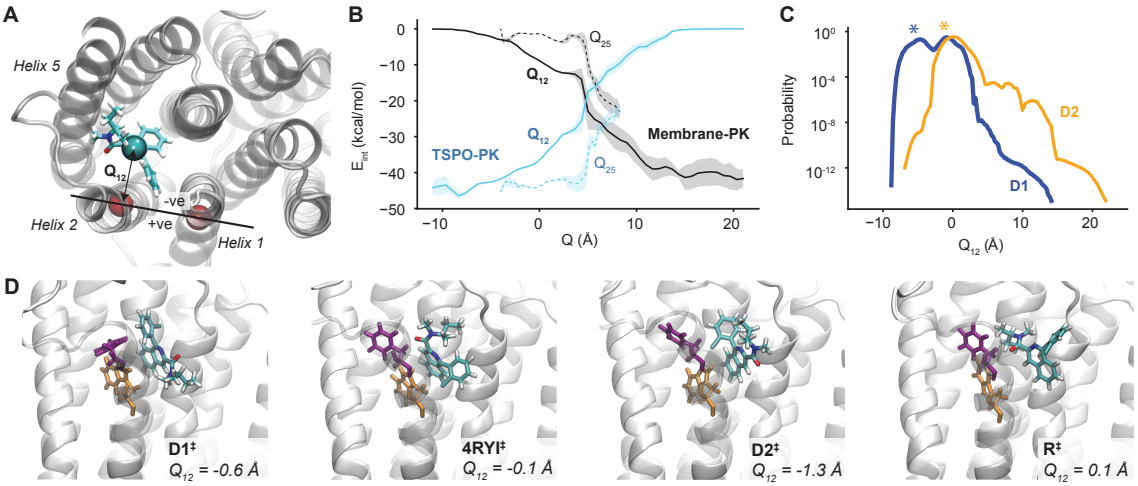

Fig. 4. Analysis of membrane-mediated exit paths. (A) The coordinate Q_{ij} is defined as the x-y distance between the center of mass of PK and the line that connects the centers of mass of helix i and helix j. LP1 is not shown here for clarity. (B) The expectation values of the interaction energy between PK and TSPO (red) and between PK and the membrane (black) are shown as a function of Q. In each case the solid line shows Q_{12} and the dashed line shows Q_{25}. The shaded region indicates the standard error over the ensemble of measurements at each Q value. (C) Probability curves projected onto Q_{12} for simulations initialized in Pose D1 (blue) and D2 (orange). Q_{12} values of the starting structures are marked with (*). (D) Poses from transition pathways with $Q \approx 0$. These poses are also labeled in the CSN of Fig. 2. Phe46 is shown in purple and Trp50 is shown in orange.

ate into the solvent via the LP1 region: it instead dissociates into the membrane. The CSN shows that all the poses, besides pose R, connect directly to the unbound states, shown in yellow and orange, where PK is fully dissolved into the lipid membrane. In all of these pathways, PK exits between TM-1 and TM-2. The pose R trajectories show two different pathways that have a moderate LASA – one between TM-1 and TM-2 and another between TM-2 and TM-5 – where PK forms direct interactions with membrane lipids. Given more simulation time, it is probable that these pathways will connect to the unbound states observed in the other poses.

By summing the weights of the unbinding trajectories, we can directly estimate the unbinding rate for each starting pose (Fig. 3). Pose D2 had a high unbinding flux and a predicted mean first passage time of unbinding (MFPT) of less than 0.02 s, indicating a clear lack of stability with respect to the other poses. Poses D3 and D4 had predicted MFPTs of 2.6 and 4.1 minutes, respectively, still lower than the experimental measurements; these estimates are likely to continue to decrease with further simulation time. Poses 4RYI and D1 had MFPT estimates near or above the experimental MFPT (28 and 260 min, respectively). No unbinding events were observed for Pose R.

We introduce the coordinate Q_{ij}, which measures the minimum x-y distance from the center of mass of the ligand to the line connecting the centers of mass of helix i and helix j (Fig. 4A). Negative Q values indicate the ligand is within the helical bundle and positive values indicate the ligand is outside the bundle. This provides a basis to compare between different pathways and a means of obtaining general information about membrane-mediated ligand unbinding pathways. Fig. 4B compares the TSPO-PK interaction energy (E_{int}) with membrane-PK interaction energy. In the Q_{12} pathway (solid lines), PK interacts more closely with the lipid membrane than TSPO after about 5 Å. For the Q_{25} pathway (dashed lines) this crossover occurs at 7.5 Å. The difference is due to the orientation of PK along the two pathways: it dissociates with its hydrophobic tail first in the Q_{12} pathway and aromatic rings first in the Q_{25} pathway (Fig. 4D).

We also measure E_{int} profiles between PK and individual residues for all residues on TM1, TM2, TM5 and LP1 (Fig. S4-S7). Early in both the Q_{12} and Q_{25} pathways, PK strongly interacts with aromatic residues Phe46 and Trp50 forming π-π interactions. These aromatic residues with long sidechains follow PK along the unbinding pathway, which is observed by plotting the Q value of individual residues as a function of Q-PK (Fig. S8 and S9). Interestingly, this phenomenon occurs for smaller amino acid sidechains as well: Gly22 and Pro47 both change Q value significantly over the Q_{12} pathway, indicating significant distention of the helices during unbinding.

The results of our simulation show that from all six initial PK poses, using the *R. sphaeroides* TSPO structure, the ligand dissociates into the membrane through the transmembrane helices. However, previous contradictory results (21) used a different starting pose and TSPO structure. One key difference is a salt bridge formed between Asp32 and Arg43 in the *R. sphaeroides* structure that stabilizes the helix in the LP1 region. This stabilization limits the freedom of motion of the LP1 loop, sterically hindering PK from leaving via the pathway observed by Bruno *et al.* (21). Additionally, the Trp50 residue is highly conserved across organisms of several species and kingdoms. It has been shown in our simulations that the aromatic rings of PK form π-π interactions with the Trp50 rings, both in the bound state and along the Q_{12} pathway. These stabilizing interactions could lower the barrier to entry for other TSPO ligands such as protoporphyrin-IX and heme, which are also largely aromatic.

PK dissociating into the membrane raises questions about membrane insertion and removal along ligand binding paths.

Additional REVO simulations with only PK and the lipid membrane could reveal the diffusion coefficient of PK in the membrane to form holistic models of membrane-mediated binding from solvent to binding site. A larger question is how the presence of other proteins known to interact with TSPO, such as VDAC (voltage dependent ion channel) (12) and cytochrome P450s (30) affect the unbinding/binding and insertion/removal pathways. Cholesterol could also affect the binding pathways of PK, either by binding to TSPO and affecting a conformational change, or through membrane fluidity, which could affect the (un)binding rate of PK as it interacts with the membrane(31). These questions could be investigated with additional simulations.

Acknowledgements

This work was supported by R01GM130794 from the National Institutes of Health. The authors thank Dr. Jens Meiler and Georg Kuenze for providing the pose R structure from Ref. (28). Note that this work has not yet been peer-reviewed.

Supplementary Material

Extended Materials and Methods as well as supplemental figures are available in the Supplementary Material.

Author Contributions

TD and AU setup the simulations; TD conducted the simulations and analysis; SFM and AD designed the project; TD, AU, SFM and AD wrote the manuscript.

Bibliography

1. Robert A. Copeland. The drug-target residence time model: a 10-year retrospective. *Nat. Rev. Drug Discov.*, 15:87–95, 2016. doi: 10.1038/nrd.2015.18.
2. Samuel D. Lotz and Alex Dickson. Unbiased Molecular Dynamics of 11 min Timescale Drug Unbinding Reveals Transition State Stabilizing Interactions. *Journal of the American Chemical Society*, 140(2):618–628, 2018. ISSN 0002-7863.
3. Alex Dickson. Mapping the Ligand Binding Landscape. *Biophysical Journal*, 115(9):1707–1719, 2018. ISSN 15420086. doi: 10.1016/j.bpj.2018.09.021.
4. Alex Dickson and Samuel D Lotz. Multiple Unbinding Pathways and Ligand-Induced Destabilization Revealed by WExplore. *Biophysical Journal*, 112:620–629, 2017.
5. Barbra Costa, Eleonora Da Pozzo, Chiara Giacomelli, Elisabetta Barresi, Sabrina Taliani, Federico Da Settimo, and Claudia Martini. Tspo ligand residence time: a new parameter to predict compound neurosteroidogenic efficacy. *Sci. Rep.*, 6(18164), 2016. doi: 10.1038/srep18164.
6. Frederick Bonsack and Sangeetha Sukumari-Ramesh. Tspo: An evolutionarily conserved protein with elusive functions. *Int. J. Mol. Sci.*, 19(1694), 2018. doi: 10.3390/ijms19061694.
7. F. Li, J. Liu, Y. Zheng, R. M. Garavito, and S. Ferguson-Miller. Crystal structures of translocator protein (tspo) and mutant mimic of a human polymorphism. *Sci.*, 347:555–558, 2015. doi: 10.1126/science.1260590.
8. Y. Guo, R. C. Kalathur, Q. Liu, R. Bruni, C. Ginter, E. Kloppmann, B. Rost, and W. A. Hendrickson. Structure and activity of tryptophan-rich tspo proteins. *Sci.*, 347:551–555, 2015. doi: 10.1126/science.aaa1534.
9. M. Jaremko, Ł. Jaremko, K. Giller, S. Becker, and M. Zweckstetter. Structure of the mitochondrial translocator protein in complex with a diagnostic ligand. *Sci.*, 343:1363–1366, 2014. doi: 10.1126/science.1248725.
10. M. Jaremko, Ł. Jaremko, K. Giller, S. Becker, and M. Zweckstetter. Structural integrity of the a147t polymorph of mammalian tspo. *Chembiochem*, 16(10):1483–1489, 2015. doi: 10.1002/cbic.201500217.
11. H. Li and V. Papadopoulos. Peripheral-type benzodiazepine receptor function in cholesterol transport. identification of a putative cholesterol recognition/interaction amino acid sequence and consensus pattern. *Endocrinology*, 139(12):4991–4997, 1998. doi: 10.1210/endo.139.12.6390.
12. Alana M. Scarf, Lars M. Ittner, and Michael Kassiou. The translocator protein (18 kda): Central nervous system disease and drug design. *J. Med. Chem.*, 52:581–592, 2009. doi: 10.1021/jm8011678.
13. L. Veenman, V. Papadopoulos, and M. Gavish. Channel-like functions of the 18-kda translocator protein (tspo): regulation of apoptosis and steroidogenesis as part of the host-defense response. *Curr. Pharm. Des.*, 13(23):2385–2405, 2007. doi: 10.2174/138161207781368710.
14. H. Batoko, V. Veljanovski, and P. Jurkiewicz. Enigmatic translocator protein (tspo) and cellular stress regulation. *Trends Biochem Sci.*, 40:497–503, 2015. doi: 10.1016/j.tibs.2015.07.001.
15. Jemma Gatliff, Daniel A. East, Aarti Singh, Maria Soledad Alvarez, Michele Frison, Ivana Matic, Caterina Ferraina, Natalie Sampson, Federico Turkheimer, and Michelangelo Campanella. A role for tspo in mitochondrial ca^{2+} homeostasis and redox stress signaling. *Cell Death Dis.*, 8:e2896, 2017. doi: 10.1038/cddis.2017.186.
16. Lan N. Tu, K. Morohaku, P. R. Manna, S. H. Pelton, W. R. Butler, D. M. Stocco, and V. Selvaraj. Peripheral benzodiazepine receptor/translocator protein global knock-out mice are viable with no effects on steroid hormone biosynthesis. *J. Biol. Chem.*, 289:27444–27454, 2014. doi: 10.1074/jbc.M114.578286.
17. Lan N. Tu, Amy H. Zhao, Douglas M. Stocco, and Vimal Selvaraj. Pk11195 effect on steroidogenesis is not mediated through the translocator protein (tspo). *Endocrinology*, 156:1033–1039, 2015. doi: 10.1210/en.2014-1707.
18. Rainer Rupprecht, Vasslilos Papadopoulos, Gerhard Rammes, Thomas C. Baghai, Jinjiang Fan, Nagaraju Akula, Ghislaine Groyer, David Adams, and Michael Schumacher. Translocator protein (18 kda) (tspo) as a therapeutic target for neurological and psychiatric disorders. *Nat. Rev. Drug Discov.*, 9:971–988, 2010. doi: 10.1038/nrd3295.
19. Mara Perrone, Byung Seook Moon, Hyun Soo Park, Valentino Laquintana, Jae Ho Jung, Annalisa Cutrignelli, Angela Lopedota, Massimo Franco, Sang Eun Kim, Byung Chul Lee, and Nunzio Denora. A novel pet imaging probe for the detection and monitoring of translocator protein 18 kda expression in pathological disorders. *Sci. Rep.*, 6(20422), 2016. doi: 10.1038/srep2042.
20. Barbra Costa, Chiara Giacomelli, Eleonora Da Pozzo, Sabrinia Taliani, Federico Da Settimo, and Claudia Martini. The anxiolytic etifoxine binds to tspo ro5-4864 binding site with long residence time showing a high neurosteroidogenic activity. *ACS Chem. Neurosci.*, 8:1448–1454, 2017. doi: 10.1021/acschemneuro.7b00027.
21. Agostino Bruno, Elisabetta Barresi, Nicola Simola, Eleonora Da Pozzo, Barbara Costa, Ettore Novellino, Federico Da Settimo, Claudia Martini, Sabrina Taliani, and Sandro Cosconati. Unbinding of translocator protein 18 kda (tspo) ligands: From in vitro residence time to in vivo efficacy via in silico simulations. *ACS Chem. Neurosci.*, 10(8):3805–3814, 2019. doi: 10.1021/acschemneuro.9b00300.
22. Fei Li, Jian Liu, Nan Liu, Leslie A. Kuhn, R. Michael Garavito, and Shelagh Ferguson-Miller. Translocator protein 18 kda (tspo): An old protein with new functions? *Biochemistry*, 55:2821–2831, 2016. doi: 10.1021/acs.biochem.6b00142.
23. Christophe Chipot, François Dehez, Jason R. Schnell, Nicole Zitzmann, Eva Pebay-Peyroula, Laurent J. Catoire, Bruno Miroux, Edmund R. S. Kunji, Gianlugi Veglia, Timothy A. Cross, and Paul Schanda. Perturbations of native membrane protein structure in alkyl phosphocholine detergents: A critical assessment of nmr and biophysical studies. *Chem. Rev.*, 118:3559–3607, 2018. doi: 0.1021/acs.chemrev.7b005.
24. Juan Zeng, Riccardo Guareschi, Mangesh Damre, Ruyin Cao, Achim Kless, Bernard Neumaier, Andreas Bauer, Alejandro Giorgetti, Paolo Carloni, and Giulia Rossetti. Structural prediction of the dimeric form of the mammalian translocator membrane protein tspo: A key target for brain diagnostics. *Int. J. Mol. Sci*, 19(2588), 2018. doi: 10.3390/ijms19092588.
25. Nazanin Donyapour, Nicole M. Roussey, and Alex Dickson. Revo: Resampling of ensembles by variation optimization. *J. Chem. Phys.*, 150(244112), 2019. doi: 10.1063/1.5100521.
26. Tom Dixon, Samuel D. Lotz, and Alex Dickson. Predicting ligand binding affinity using on- and off-rates for the sampl6 sampling challenge. *J. Comput. and Mol Des.*, 32:1001–1012, 2018. doi: 10.1007/s10822-018-0149-3.
27. Richard A. Friesner, Jay L. Banks, Robert B. Murphy, Thomas A. Halgren, Jasna J. Klicic, Daniel T. Mainz, Matthew P. Repasky, Eric H. Knoll, Mee Shelley, Jason K. Perry, David E. Shaw, Perry Francis, and Peter S. Shenkin. Glide: A new approach for rapid, accurate docking and scoring. 1. method and assessment of docking accuracy. *J. of Med. Chem.*, 47(7):1739–1749, 2004. doi: 10.1021/jm0306430.
28. Yan Xia, Kaitlyn Ledwitch, Georg Kuenze, Amanda Duran, Jun Li, Charles R. Sanders, Charles Manning, and Jems Meiler. A unified structural model of the mammalian translocator protein (tspo). *J. Biomol. NMR*, 73:347–364, 2019. doi: 10.1007/s10858-019-00257-1.
29. Sunhwan Jo, Taehoon Kim, Vidyashankara G. Iyer, and Wonpil Im. Charmm-gui: a web-based graphical user interface for charmm. *J. of Comput. Chem.*, 29:1859–1865, 2008. doi: 10.1002/jcc.20945.
30. Andrew Midzak, Nagaraju Akula, Laurent Lecanu, and Vassilos Papadopoulos. Novel androstenetriol interacts with the mitochondrial translocator protein and controls steroidogenesis. *J. Biol. Chem.*, 286:9875–9887, 2011. doi: 10.1074/jbc.M110.203216.
31. Garima Jaipuria, Andrei Leonov, Karin Giller, Suresh Kumar Vasa, Łukasz Jaremko, Mariusz Jaremko, Rasmus Linser, Stefan Becker, and Markus Zweckstetter. Cholesterol-mediated allosteric regulation of the mitochondrial translocator protein structure. *Nat. Commun.*, 8(14893), 2017. doi: 10.1038/ncomms14893.